Research Article Vol. 9, No. 11 / November 2022 / Optica 1289

Temporal trapping: a route to strong coupling and deterministic optical quantum computation

Ryotatsu Yanagimoto,[1,*] Edwin Ng,[1,2] Marc Jankowski,[1,2] Hideo Mabuchi,[1] and Ryan Hamerly[2,3,4]

[1]E. L. Ginzton Laboratory, Stanford University, Stanford, California 94305, USA
[2]Physics & Informatics Laboratories, NTT Research, Inc., Sunnyvale, California 94085, USA
[3]Research Laboratory of Electronics, MIT, 50 Vassar Street, Cambridge, Massachusetts 02139, USA
[4]e-mail: rhamerly@mit.edu
*Corresponding author: ryotatsu@stanford.edu

Received 18 August 2022; revised 13 October 2022; accepted 14 October 2022; published 17 November 2022

The realization of deterministic photon–photon gates is a central goal in optical quantum computation and engineering. A longstanding challenge is that optical nonlinearities in scalable, room-temperature material platforms are too weak to achieve the required strong coupling, due to the critical loss-confinement trade-off in existing photonic structures. In this work, we introduce a spatio-temporal confinement method, dispersion-engineered temporal trapping, to circumvent the trade-off, enabling a route to all-optical strong coupling. Temporal confinement is imposed by an auxiliary trap pulse via cross-phase modulation, which, combined with the spatial confinement of a waveguide, creates a "flying cavity" that enhances the nonlinear interaction strength by at least an order of magnitude. Numerical simulations confirm that temporal trapping confines the multimode nonlinear dynamics to a single-mode subspace, enabling high-fidelity deterministic quantum gate operations. With realistic dispersion engineering and loss figures, we show that temporally trapped ultrashort pulses could achieve strong coupling on near-term nonlinear nanophotonic platforms. Our results highlight the potential of ultrafast nonlinear optics to become the first scalable, high-bandwidth, and room-temperature platform that achieves strong coupling, opening a path to quantum computing, simulation, and light sources.

https://doi.org/10.1364/OPTICA.473276

1. INTRODUCTION

Photons are ideal carriers of quantum information, enjoying minimal decoherence even at room temperature and propagating long distances with low loss at high data rates. These advantages render optics essential to quantum key distribution [1], networking [2], and metrology [3,4], and have led to significant progress towards optical quantum computation [5–7]. The main challenge to the latter lies in realizing on-demand entangling gates between optical qubits, in light of the weak photon–photon coupling in most materials. The dominant paradigm—linear optical quantum computing (LOQC)—circumvents this problem via the inherent nonlinearity of measurements [8], but as the resulting gates are probabilistic [9], LOQC relies on the creation of entangled ancillae [8] or cluster states [10–12], which suffer from large resource overheads in terms of the number of photons and detectors per gate [13–16].

The inherent difficulty of probabilistic gates has fueled sustained interest in so-called nonlinear-optical quantum computing (NLOQC), where deterministic gate operations are implemented coherently through a nonlinear-optical interaction [17,18]. Here, high-fidelity gates are possible in the strong-coupling regime when the nonlinear interaction rate g exceeds the decoherence rate κ, i.e., $g/\kappa \gg 1$. Strong coupling is readily achieved in cavity QED, where resonant two-level systems such as atoms mediate strong optical nonlinearities [19–23], but such systems require vacuum and/or cryogenic temperatures, and challenges with fabrication, yield, and noise remain daunting despite decades of research. By contrast, bulk material nonlinearities such as $\chi^{(3)}$ and $\chi^{(2)}$ are robust, scalable, and room temperature, but the optical interaction is much weaker, imposing very demanding requirements on the optical loss (quality factor Q) and confinement (mode volume V). Moreover, to support nonlinear interactions among multiple frequency bands, e.g., in $\chi^{(2)}$ systems, one has to overcome the challenge of realizing high-Q resonances separated by a large frequency, for which guided-wave (e.g., ring, disk) resonators are favorable options compared to photonic crystal (PhC) cavities. Great progress has been achieved to this end in ultralow-loss thin-film $LiNbO_3$ (TFLN) [24,25] and indium gallium phosphide (InGaP) nanophotonics [26], which has rendered plausible a near-strong coupling regime $g/\kappa \sim 1$ with ring resonators in the near future. Even with these developments, however, $g/\kappa \gg 1$ remains a challenge owing to the ring's large mode volume, as the axial dimension remains unconfined. To reach strong coupling, field confinement in the transverse dimensions is not enough. We also need a means to confine light in the third direction—time.

This paper introduces the *temporal trap*, a nonlinear-optical mechanism to confine light in time as well as space. To facilitate trapping, a strong non-resonant "trap pulse," which co-propagates with the target fields, introduces a nonlinear phase shift through cross-phase modulation (XPM). Analogous to an optical soliton [27], the trap pulse creates a flying photonic cavity that supports a bound mode formed by the competition between dispersion and nonlinearity, with a mode volume reduced by the trap duty cycle. With appropriate dispersion engineering [28], the bound mode is strongly detuned from the remaining cavity degrees of freedom, ensuring single-mode dynamics that circumvent the inherent challenges of pulsed nonlinear quantum gates highlighted in Refs. [29,30]. As a result, we show that high-fidelity two-qubit entangling gate (i.e., controlled-Z gate) operation is possible, providing a roadmap to fully deterministic NLOQC. The tight temporal confinement also significantly increases nonlinear coupling strength, with $g/\kappa \gtrsim 10$ plausible for realistic nonlinearities and propagation losses on TFLN photonics. While we focus on $\chi^{(2)}$ systems as a case study in this work, our proposal is generic and compatible with existing proposals in NLOQC using $\chi^{(3)}$ nonlinear interactions as well [17,18,31], where it both provides a means to resolve the otherwise unavoidable multimode interactions and also enhances nonlinear coupling strength. Additionally, our prescription using temporal traps supports time multiplexing [32,33], enabling significant parallelism in a single cavity.

2. OPTICAL QUANTUM COMPUTING IN A TEMPORAL TRAP

Single-photon qubits are a leading approach for optical quantum computation [7]. The dual-rail basis, which encodes a state in polarization [34], time-bin [35], or path [36,37], is a particularly attractive choice, since all single-qubit gates reduce to linear optics [Fig. 1(a)]. To complete the gate set, we also need a two-qubit entangling gate, e.g., a controlled-Z (CZ) gate. The most common prescription, shown in Fig. 1(b), implements CZ with a Mach–Zehnder interferometer (MZI) that encloses a Kerr-phase interaction:

$$\hat{U}_\pi[c_0|0\rangle + c_1|1\rangle + c_2|2\rangle] = c_0|0\rangle + c_1|1\rangle - c_2|2\rangle, \quad (1)$$

where $|n\rangle$ represents the n-photon Fock state. This circuit exploits the Hong–Ou–Mandel effect [38] to ensure that two photons are incident on the $\hat{U}_\pi$ gate only when the qubits are in the logical state $|\tilde{1}\tilde{1}\rangle$, implementing the π-phase shift exclusively for this state.

To implement $\hat{U}_\pi$ [Fig. 1(c)], one can employ the Knill–Laflamme–Milburn (KLM) scheme, which forms the basis for LOQC [8,9]. KLM suffers from a low success probability of 2/27 for the CZ gate, and deterministic operations require the preparation of an initial highly entangled state, e.g., a cluster state [10,11], at significant overhead [14]. In light of these difficulties, here we focus on NLOQC, which aims at deterministic gate operations using coherent nonlinear dynamics [17,18]. For instance, unitary evolution under a single-mode Kerr nonlinearity $\hat{H}_{\text{gate}} = \frac{1}{2}\chi\hat{a}^{\dagger 2}\hat{a}^2$ for time $t_\pi = \pi\chi^{-1}$ implements $\hat{U}_\pi$. In this work, we instead consider a single-mode degenerate $\chi^{(2)}$ Hamiltonian:

$$\hat{H}_{\text{gate}} = \frac{g}{2}(\hat{a}^2\hat{b}^\dagger + \hat{a}^{\dagger 2}\hat{b}), \quad (2)$$

where $\hat{a}$ and $\hat{b}$ are annihilation operators for the fundamental (FH) and second harmonic (SH) modes, respectively. As shown in Fig. 1(d), the Hamiltonian Eq. (2) mediates interactions between the two-photon FH state $|20\rangle$ and the single-photon SH state $|01\rangle$ with coupling strength $g > 0$, resulting in a Rabi oscillation between these two states. Importantly, for an initial state of $|20\rangle$, the system oscillates back to the same state after a period of

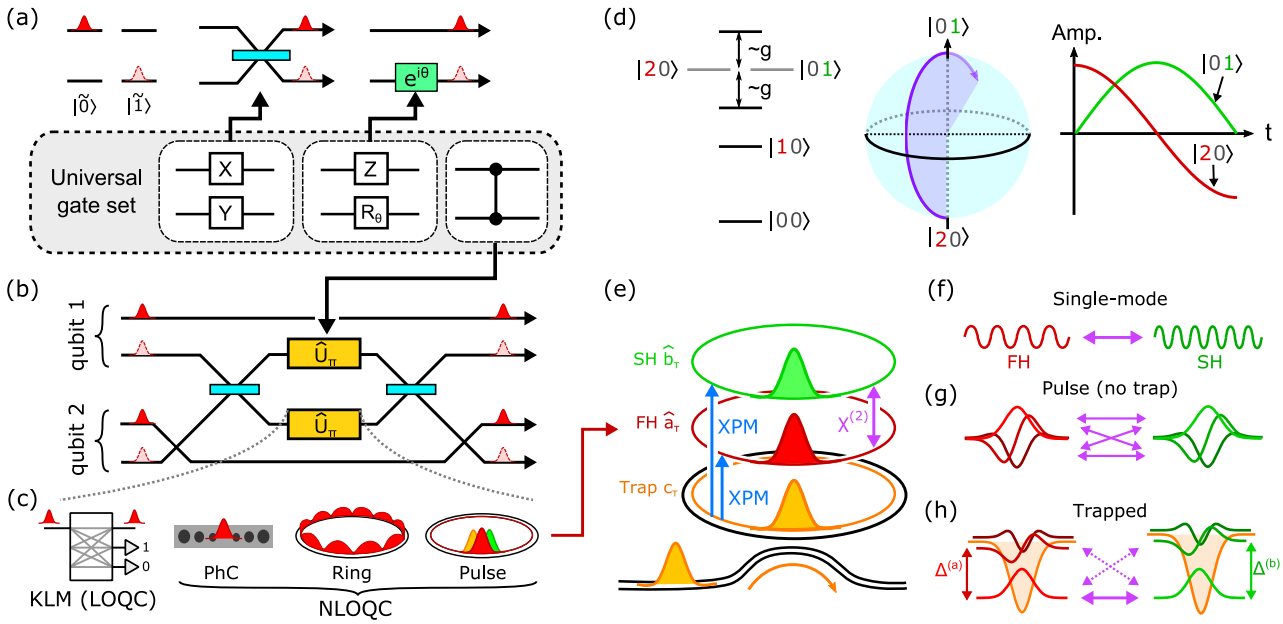

Fig. 1. Universal QC is realized on a dual-rail qubit basis with (a) single-qubit gates based on passive linear optics and (b) a CZ gate constructed from a Kerr-phase interaction $\hat{U}_\pi$ inside a Mach–Zehnder interferometer. (c) Potential realizations of $\hat{U}_\pi$ in LOQC and NLOQC. (d) $\chi^{(2)}$-mediated $\hat{U}_\pi$ gate: coupling between the FH state $|20\rangle$ and the SH state $|01\rangle$ leads to Rabi oscillations, imparting a nonlinear phase shift on the signal field. (e) Temporal trap: the $\chi^{(2)}$ interaction between FH and SH fields is enhanced when confined to ultrashort pulses through trap-pulse XPM. Untrapped dynamics are either (f) cw and single-mode or (g) pulsed and multimode, depending on the dispersion. (h) Temporal trapping imposes single-mode dynamics by breaking the degeneracy between trapped and untrapped modes, the former protected by an energy gap Δ.

$t_\pi = \sqrt{2}\pi g^{-1}$ with *an opposite sign*, i.e., $-|20\rangle$. As a result, for an initial FH state of $c_0|0\rangle + c_1|1\rangle + c_2|2\rangle$ and a vacuum pump state, unitary evolution under Eq. (2) for time t_π implements $\hat{U}_\pi$ deterministically. Such a nonlinear-optical implementation of $\hat{U}_\pi$ is also considered in Refs. [18,39–41], which motivates us to employ this as a reference protocol for evaluating the performance of our proposal.

Now, the problem of implementing a CZ gate reduces to the realization of the single-mode $\chi^{(2)}$ Hamiltonian Eq. (2) with strong coupling, for which we sketch three possible realizations in Fig. 1(c): a PhC cavity, a micro-ring resonator, and our proposed scheme using an ultrashort pulse. For resonators, the cooperativity figure of merit $g/\kappa = g/\sqrt{\kappa_a \kappa_b}$ depends on the Q factor and mode volume as follows:

$$\frac{g}{\kappa} = \sqrt{\frac{4\pi\hbar c\, d_{\text{eff}}^2}{n^3 \epsilon_0 \lambda^4} \frac{Q_a\, Q_b}{\tilde{V}}}, \tag{3}$$

where n is the refractive index of the medium, and $\tilde{V} = V/(\lambda/n)^3$ is the normalized volume, with $V = |n^3 \int E_b^*(E_a)^2 \mathrm{d}^3\vec{x}|^{-2}$ defined in terms of the mode overlap integral between FH and SH modes. Effective quadratic susceptibility of the medium d_{eff} is related to the native quadratic susceptibility d_{33} via $d_{\text{eff}} = d_{33}$ and $d_{\text{eff}} = (2/\pi)d_{33}$ for critical phase matching and quasi-phase matching, respectively (see Supplement 1 for details).

Table 1 reveals the trade-off between Q and V in resonator design. In terms of their generic properties, a PhC cavity leverages a wavelength-scale mode volume $V \lesssim (\lambda/n)^3$ with modest $Q \sim 10^6$ ($Q \sim 10^7$ is in principle possible, but at low yield [42–48]). However, as PhCs rely on Bragg scattering for confinement, simultaneous resonance of octave-spanning modes is very difficult, leading to lower quality factors $Q \lesssim 10^4$ at the SH [49–52]. On the other hand, the light in ring resonators is guided by total internal reflection, a geometric effect that is only weakly wavelength dependent. Therefore, rings can readily resonate modes spanning an octave, with Q factors limited only by waveguide loss. With ion-sliced TFLN, losses of 3 dB/m ($Q = 10^7$) have been achieved [24], and there is a pathway to reach $Q = 10^8$ with process improvements [53–55], which is close to the bulk material limit [56–59]. For the Kerr effect, PhC cavities offer better performance; however, the native nonlinearity is still too weak in standard materials to observe strong coupling with reasonable cavity designs (see Supplement 1). More sophisticated engineering methods, e.g., coherent photon conversion [18,60], could provide further enhancement to the nonlinearities on $\chi^{(3)}$ platforms. For $\chi^{(2)}$, ring resonators are the superior option. Recent experiments have demonstrated $g/\kappa \sim 0.01$ on ultralow-loss TFLN [25] and InGaP [26] micro-ring resonators; however, the strong-coupling regime $g/\kappa \gg 1$ remains challenging due to the ring's large mode volume.

Table 1. Typical Estimates of Q, V, and Cooperativity for Competing Confinement Mechanisms[a]

	Q_a	Q_b	$\tilde{V}$	d_{eff}	g/κ	Modes
PhC[b]	10^6	10^3	1	33 pm/V	0.03	1
Ring[c]	10^7	10^7	2000	21 pm/V	0.1	1
Pulse[d]	10^7	10^7	40	21 pm/V	0.8	$\gg 1$

[a]$LiNbO_3$, $\lambda = 1.55$ μm.
[b]Doubly-resonant PhC based on intersecting nanobeams, BIC, or nanopillars [49–52].
[c]Ring circumference 2 mm, quasi-phase-matched $d_{\text{eff}} = (2/\pi)d_{33}$, loss $\alpha =$ 3 dB/m, and $Q = 5 \times 10^6$ at $\lambda = 1.59$ μm [24].
[d]Pulse of width 100 fs, dispersion engineered waveguide.

This paper studies the third approach: nonlinear enhancement with trapped pulses. The approach is shown in Fig. 1(e), where in addition to the resonant FH and SH fields, we introduce a nonresonant "trap" field, generated by an external pulse train, which forms a temporal potential for the resonant, quantum modes. The Hamiltonian for this system takes the form [61]

$$\hat{H} = \underbrace{\frac{r}{2}\int \mathrm{d}\tau \left(\hat{a}_\tau^{\dagger 2}\hat{b}_\tau + \hat{a}_\tau^2 \hat{b}_\tau^\dagger\right)}_{\hat{H}_{\text{NL}}} + \sum_{u\in\{a,b\}} \underbrace{\int \mathrm{d}\tau\, \hat{u}_\tau^\dagger G_u(\tau)\hat{u}_\tau}_{\hat{H}_{a,\text{L}}, \hat{H}_{b,\text{L}}}, \tag{4}$$

with periodic boundary conditions on $-T/2 \le \tau \le T/2$, where T is the cavity round-trip time (see Supplement 1).

Here, $\hat{a}_\tau$ and $\hat{b}_\tau$ are, respectively, FH and SH field operators with commutation relations $[\hat{a}_\tau, \hat{a}_{\tau'}^\dagger] = [\hat{b}_\tau, \hat{b}_{\tau'}^\dagger] = \delta(\tau - \tau')$, defined in terms of the fast-time coordinate τ [62] in a co-propagating frame synchronous with the trap field. $\hat{H}_{\text{NL}}$ represents the $\chi^{(2)}$ interaction, while $\hat{H}_{a,\text{L}}$ and $\hat{H}_{b,\text{L}}$ are the respective linear terms for the FH and SH. For the latter, $G_u(\tau) = D_u(-\mathrm{i}\partial_\tau) + V_u(\tau)$ is a function of the dispersion operator D_u and the trap potential V_u, with $u \in \{a, b\}$. The $\chi^{(2)}$ nonlinear coupling constant $r = v_g\sqrt{\hbar\omega_{b,0}\eta_0}$ is related to group velocity v_g, SH frequency $\omega_{b,0}$, and normalized SH generation (SHG) efficiency η_0 with units [power^{-1} · length^{-2}]. As the trapping potential is mediated by XPM, the shape of the temporal trap $V_u(\tau) = -(n_2/n)\omega_u$, $0|c_\tau|^2/A$ is determined by the signal frequency ω_u, 0, trap-pulse power $|c_\tau|^2$, nonlinear index n_2, and mode area A. Taking into account dispersion up to second order and assuming group velocity matching between FH and SH, $D_u(s) = \omega_{u,0} - \frac{1}{2}(\beta_{u,2}/\beta_1)s^2$, where the first and second terms represent the carrier frequency and group velocity dispersion (GVD), respectively. The eigenstates of $\hat{H}_{u,\text{L}}$ consist of excitations of normal modes $\Psi_{u,m}(\tau)$ governed by competition between the trap-pulse XPM and GVD, and they are found by solving an eigenmode problem:

$$\underbrace{\left(\omega_{u,0} + \frac{\beta_{u,2}}{2\beta_1}\partial_\tau^2 + V_u(\tau)\right)}_{G_u(\tau)} \Psi_{u,m}(\tau) = \lambda_{u,m}\Psi_{u,m}(\tau). \tag{5}$$

In the absence of a trap ($V_u(\tau) = 0$), Eq. (5) admits continuous wave (cw) eigenmodes $\Psi_{u,m}(\tau) \propto e^{2\pi i m\tau/T}$, i.e., the usual normal modes of a cavity. In a typical nanophotonic cavity with nonvanishing $\beta_{u,2}$ [Fig. 1(f)], large energy gaps ($\propto \beta_{u,2}T^{-2}$) between eigenmodes ensure that the nonlinear dynamics involve only a single FH/SH mode pair [25]. This scenario properly realizes Hamiltonian Eq. (2), but with weak coupling strength due to the large mode volume. Conversely, appropriate dispersion engineering to achieve $\beta_{u,2} \approx 0$ [Fig. 1(g)] makes all modes nearly degenerate, allowing the cavity to support ultrashort pulses. However, this modal degeneracy leads to a major problem: although the nonlinear coupling is increased by the pulse confinement, $\hat{H}_{\text{NL}}$ is generally all-to-all, as no mechanism imposes a target pulse shape, leading to intrinsically multimode dynamics unsuitable for high-fidelity qubit operations [29,30]. These limits highlight the trade-offs between gate fidelity and coupling rate in $\chi^{(2)}$ resonators driven by pulses. Resonators with

large $\beta_{u,2}$ driven by long pulses may realize high-fidelity gates with low coupling rates, and conversely, resonators with small $\beta_{u,2}$ driven by short pulses may realize large coupling rates at the cost of reduced gate fidelities. The trap potential eliminates these trade-offs between gate fidelity and coupling rate [see Fig. 1(h)]: with anomalous dispersion $\beta_{u,2} < 0$, Eq. (5) admits at least one *bound eigenmode* $\Psi_{u,0}$, localized in time and protected by an energy gap $\Delta_u = |\lambda_{u,1} - \lambda_{u,0}|$. As a result, all spurious couplings to higher-order eigenmodes are suppressed as off-resonance (i.e., phase-mismatched), and the single-mode dynamics of Eq. (2) are recovered, but with a nonlinear coupling boosted by the temporal confinement of $\Psi_{u,0}$.

The importance of single-mode dynamics to high-fidelity gate operation is highlighted in Fig. 2, where we show the propagation of a signal instantiated in a two-photon FH pulse $|20\rangle = 2^{-1/2}(\hat{a}^\dagger)^2|0\rangle$, where $\hat{a} = \int d\tau \Psi^*(\tau)\hat{a}_\tau$ is the annihilation operator for mode $\Psi(\tau)$. To illustrate the limitations of the untrapped case, we first implement $\hat{U}_\pi$ using an input Gaussian waveform $\Psi(\tau)$ with $V_u(\tau) = 0$. Here, the pulse width and chirp are chosen to maximize the gate fidelity given a finite gate time (see Supplement 1), but we observe a rapid decay of Rabi oscillations even for such optimized pulse parameters [see Fig. 2(b)]. This observed leakage out of the computational subspace is due to the intrinsically multimode structure of the nonlinear polarization, which couples photons into parasitic temporal modes. These results provide evidence that generic quantum nonlinear propagation of a pulse cannot be described by a single-mode model such as Eq. (2), posing a nontrivial challenge for NLOQC. This problem is often overlooked in the community, with most proposals assuming a single-mode model without discussing how single-mode interactions are implemented [17,18,63,64].

Turning on the temporal trap resolves this problem, restoring effective single-mode dynamics. To show this, we consider the case of a soliton trap $V_a(\tau) = V_b(\tau)/2 = -(|\beta_{a,2}|/\beta_1\tau_0^2)\mathrm{sech}^2(\tau/\tau_0)$ with width τ_0, which supports a single bound mode $\Psi_{a,0} = \Psi_{b,0} = (2\tau_0)^{-1/2}\mathrm{sech}(\tau/\tau_0)$. Here, the finite energy gap $\Delta_a = \Delta_b/2 = |\beta_{a,2}|/2\beta_1\tau_0^2$ protects the computational subspace spanned by the bound modes from decoherence, acting as a phase mismatch (i.e., detuning) that prevents the nonlinear polarization induced by each bound mode from driving continuum modes. For simplicity, we have assumed the dispersion relationships $\beta_{a,2} = \beta_{b,2}/2$ in this work, but departure from this condition does not qualitatively change the results. The $\chi^{(2)}$ interaction between the FH and SH bound modes becomes phase-matched (i.e., resonant) when $\omega_{b,0} - 2\omega_{a,0} = 0$, which can be achieved, e.g., by temperature tuning. As a result, effectively single-mode physics reproducing Eq. (2) is realized between the bound FH and SH modes with the coupling constant given by

$$g = \frac{\pi r}{4\sqrt{2\tau_0}}, \tag{6}$$

which scales as $\tau_0^{-1/2}$ (see Supplement 1). In Fig. 2(a), we show the evolution of a two-photon state instantiated in the FH bound mode, where the photons in the trap are well localized and propagate without dispersing apart from an initial transient. In addition, the dynamics of the SH [Fig. 2(b)] exhibit near-complete Rabi oscillations even for a modest trap with $\Delta/g = 1$, where $\Delta = \Delta_a = \Delta_b/2$. These high-contrast oscillations provide strong evidence of effective single-mode dynamics, which can be further quantified as follows. Ideally, the gate dynamics are confined within the computational subspace spanned by $|20\rangle = 2^{-1/2}(\hat{a}^\dagger)^2|0\rangle$ and $|01\rangle = \hat{b}^\dagger|0\rangle$, so we can directly project the system evolution onto span($|20\rangle$, $|01\rangle$) in Fig. 2(c). The fact that nearly all of the state amplitude remains in the subspace implies that we have realized the desired single-mode dynamics, i.e., a 180° rotation in the Bloch sphere, picking up a π phase shift after returning to the initial state $|20\rangle$.

Gate fidelity scales favorably even for moderate trap depths. In Fig. 2(d), we plot the error $\mathcal{E}$ of a CZ gate as a function of the gap, showing a favorable scaling of $\mathcal{E} \propto (\Delta/g)^{-2}$. For a reference input state, we observe that gate operation with fidelity >99% is possible with $\Delta/g \gtrsim 3$. To visualize the nature of the gate errors, we also

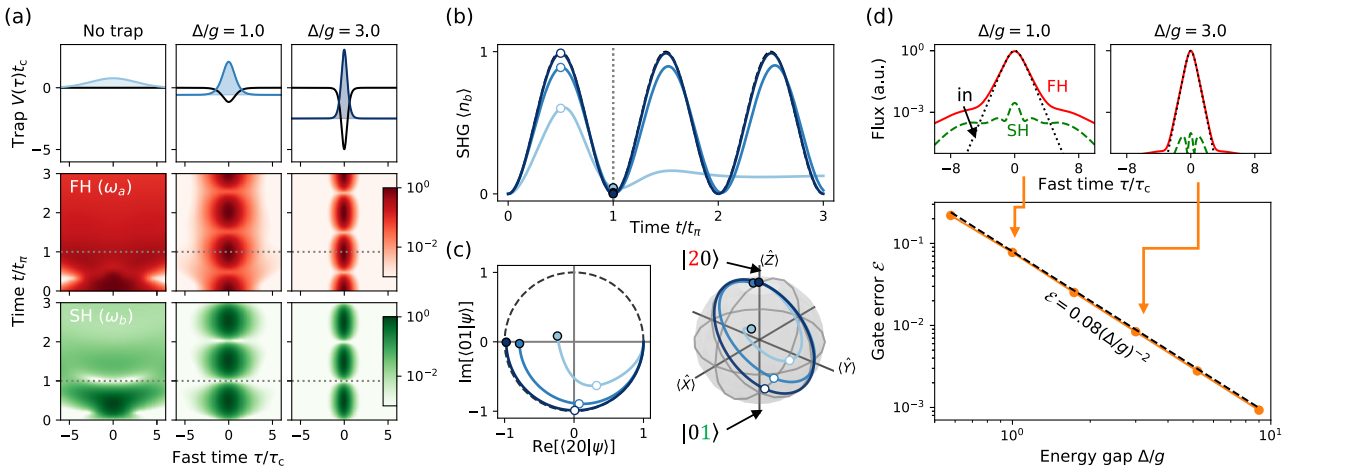

Fig. 2. Two-photon Kerr-phase gate $\hat{U}_\pi$ with and without temporal trap acting on an initial two-photon FH state $|20\rangle$: (a) initial state and FH/SH power $\langle\hat{a}_\tau^\dagger\hat{a}_\tau\rangle$, $\langle\hat{b}_\tau^\dagger\hat{b}_\tau\rangle$ as a function of time. (b) Rabi oscillations visualized in terms of the total SH photon number as well as (c) a Hilbert-space projection onto span($|20\rangle$, $|01\rangle$) and rotations on the pseudo-Bloch sphere characterized by the pseudo-Pauli operators $\hat{X} = (\hat{a}^{\dagger 2}\hat{b} + \hat{a}^2\hat{b}^\dagger)/\sqrt{2}$, $\hat{Y} = (\hat{a}^{\dagger 2}\hat{b} - \hat{a}^2\hat{b}^\dagger)/\sqrt{2}i$, $\hat{Z} = \frac{1}{2}\hat{a}^{\dagger 2}\hat{a}^2 - \hat{b}^\dagger\hat{b}$ (these project onto Pauli matrices in the two-state subspace). Here we subtract trivial phase rotations induced by the linear dynamics; see Supplement 1. (d) Gate error of a CZ gate acting on a reference state $\frac{1}{2}(|\tilde{0}\rangle + |\tilde{1}\rangle)_1 \otimes (|\tilde{0}\rangle + |\tilde{1}\rangle)_2$ as a function of the energy gap Δ/g, where subscripts represent the index of qubits. Insets show deviation of output field from the target (input) FH waveform. For all simulations, we use $\beta_{2,a} = \beta_{2,b}/2$ and $\omega_{b,0} - 2\omega_{a,0} = 0$ with a large enough system size T to avoid boundary effects. See Supplement 1 for a full discussion on numerical simulations.

show the temporal distribution of the photons; for a shallow trap, photons leak out as dispersive waves, which effectively act as decoherence channels, and incomplete conversion leads to residual SH power. Deepening the trap increases the confinement to the bound mode, suppressing these dispersive waves. Further, the interaction time $t_\pi \propto \tau_0^{-1/2}$ required to implement the gate also shortens for larger trap depth.

3. DISPERSION ENGINEERING AND EXPERIMENTAL PROSPECTS

Having established that temporal trapping enables high-fidelity quantum gates with enhanced coupling rates, we now discuss the prospects for experimental realizations in presently available nanophotonics platforms. In realistic situations, photon loss is the primary decoherence channel for quantum gate operations, and to achieve high gate fidelity, the nonlinear coupling rate g has to be larger than the characteristic loss rate κ, which we define as the geometric mean of the FH and SH losses $\kappa = \sqrt{\kappa_a \kappa_b}$. This choice is motivated by analogy to the cooperativity $C \propto g^2/\kappa_{\text{cavity}}\gamma_{\text{atom}}$ in cavity QED systems [65].

For a ring resonator, the nonlinear coupling between the nominal cw modes is

$$g_{\text{cw}} = \frac{v_g\sqrt{\hbar\omega_{b,0}\eta_0}}{\sqrt{T}}, \tag{7}$$

where we have used $r = v_g\sqrt{\hbar\omega_{b,0}\eta_0}$. The round-trip length of the resonator is given by $L = v_g T$, and a smaller L enhances g_{cw} via tighter modal confinement. While micro-ring resonators with radii $\lesssim 100\ \mu\text{m}$ have been realized, bending losses make it challenging to significantly reduce the mode volume further, limiting g_{cw} to the order of few megahertz. The same limitation exists for whispering-gallery-mode resonators (WGMRs). While PhC cavities can realize much smaller wavelength-scale modal confinement and thus stronger coupling, it is challenging to realize high-Q resonances spanning over an octave, which compromises the overall loss κ and results in g/κ similar in order of magnitude to ring resonators.

In this context, our prescription allows us to circumvent this trade-off between the mode volume and the loss: the temporal trap forms a smaller "flying cavity" inside a ring resonator, which confines the light further in the axial (temporal) dimension, so that nonlinear interactions between photons benefit from both small mode volume and low loss. Specifically, the nonlinear coupling of the temporally trapped pulses takes the form

$$g_{\text{trap}} = \frac{\pi v_g\sqrt{\hbar\omega_{b,0}\eta_0}}{4\sqrt{2\tau_0}} = \frac{\pi}{4\sqrt{2}}\sqrt{T/\tau_0}\,g_{\text{cw}}, \tag{8}$$

where the width of the trap τ_0 plays the role of the size of an effective cavity. Comparing g_{trap} to the cw coupling rate of the same resonator, we find that the coupling is enhanced by the factor proportional to the square root of the pulse duty cycle. Because g_{trap} is independent of T, temporal trapping may realize large coupling rates for resonators of arbitrary length.

For concreteness, Fig. 3 shows a design of a TFLN resonator optimized for implementing our scheme. To couple the quantum states in and out of the resonator with high efficiency, we assume that the coupling between the resonator and the bus waveguide is dynamically controlled, e.g., via nonlinear optical processes [66–68]. There exist multiple possible implementations of dynamical coupling [69–72] (potentially with their own geometrical constraints and loss considerations), so we keep the following discussions independent of the specific realization. The resonator simultaneously supports a group velocity matched FH ($\lambda_a = 1560$ nm), SH ($\lambda_b = 780$ nm), and trap pulse ($\lambda_{\text{trap}} = 2494$ nm). The GVD of both of the harmonics are designed to be anomalous, supporting localized bound modes using bright-pulse XPM. The minimum trap width τ_0 is limited by the dispersion of the trap pulse, for which we assume $\tau_0 = 100$ fs to ensure the pulse waveform does not disperse over the propagation through the trapping region. With an estimated

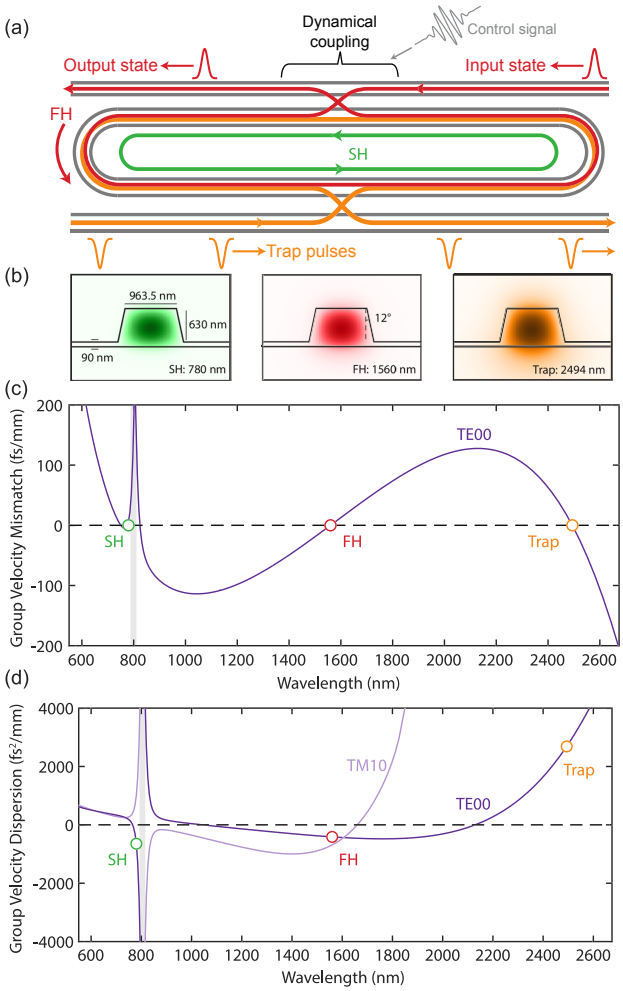

Fig. 3. Design of a microresonator implementing $\hat{U}_\pi$ with a temporal trap. (a) The FH and trap are coupled into and out of the cavity though two bus waveguides. We assume that the trap pulse is renewed in every round trip, and that quantum input/output states are switched in and out from the cavity by dynamical coupling [69–72]. (b) Waveguide geometry and TE00 field distributions associated with each interacting wave; SH (780 nm), FH (1560 nm), and trap pulse (2494 nm). (c), (d) Group velocity mismatch ($\beta_1 - \beta_{1,a}$) and group velocity dispersion (β_2) as a function of wavelength. Shaded gray region: avoided crossing between TE00 and TM10 modes. With a suitable choice of waveguide geometry, we may realize both group velocity matching between the FH and SH, and anomalous dispersion for both harmonics. For the ridge geometries considered here, anomalous dispersion may occur at short wavelengths by choosing the location of the avoided crossing to be red-detuned from the SH.

SHG efficiency of $\eta_0 = 40\ \mathrm{W^{-1}cm^{-2}}$, we obtain a coupling rate of $g_{\mathrm{trap}}/2\pi = 11.7$ MHz. For a 2 mm ring cavity ($T \approx 15$ ps), this is an order larger than the corresponding g_{cw} obtained without trapping. Moreover, the energy gap of $\Delta/g \approx 40$ provides sufficient isolation of the trapped modes from the continuum. Regarding the loss, $\alpha = 0.7\ \mathrm{m^{-1}}$ [3 dB/m] has been achieved in TFLN [24], which through the relation $\kappa = \alpha v_g$ corresponds to $\kappa/2\pi = 14.4$ MHz. These numbers highlight the potential to reach a near-strong-coupling regime $g/\kappa \sim 1$ using ultrashort pulses with technologies available at present. Note that temporal trapping has allowed us to employ a reasonably large resonator size that minimizes the bending loss and sidewall roughness loss, which we expect to make it easier to achieve the loss figure assumed above. Even with propagation loss of 30 dB/m (corresponding to $g_{\mathrm{cw}}/\kappa \sim 0.01$), we can achieve $g/\kappa \sim 0.1$.

Further improvements to g/κ may be possible in next-generation devices by leveraging the scaling of g with both ω and τ_0, and by improvements to fabrication processes to reach the material-limited loss rates for κ. Reductions of the GVD associated with the FH, SH, and trapping pulse enable corresponding reductions of trap pulse duration τ_0, thereby enhancing g_{trap}. Ultimately, few-cycle operation ($\tau_0 \approx 4\pi/\omega_{\mathrm{trap}}$) may be made possible with new approaches to dispersion engineering that reduce the GVD of the trapping pulse. Short-wavelength operation increases g_{trap} through both the explicit $\omega_{b,0}^{1/2}$ scaling of g_{cw} and the $\eta_0 \sim \omega^4$ [28] scaling associated with the tighter transverse confinement attainable at shorter wavelengths. Recent demonstrations include $\eta_0 = 330\ \mathrm{W^{-1}cm^{-2}}$ in a TFLN waveguide at $\lambda_b = 456.5$ nm [73], and in principle, devices with $\eta_0 > 1000\ \mathrm{W^{-1}cm^{-2}}$ are possible for FH pulses centered around Ti:sapphire wavelengths [28]. Moreover, the pulse width can be made shorter with a shorter wavelength, i.e., $\tau_0 \sim \omega^{-1}$, amounting to a favorable scaling of $g_{\mathrm{trap}} \sim \omega^3$. Assuming $\lambda_b = 400$ nm, which we choose to be below the Urbach tail associated with the material bandgap [74], these scalings anticipate the possibility to achieve $g_{\mathrm{trap}}/2\pi = 184$ MHz, corresponding to $g/\kappa > 10$.

In addition, process improvements may reduce losses from the present 3–6 dB/m [24,75] by more than an order of magnitude [53–55], limited primarily by bulk material absorption [56–59,76]. For known absorption-limited losses of $0.01\ \mathrm{m^{-1}}$, $0.04\ \mathrm{m^{-1}}$, and $1\ \mathrm{m^{-1}}$ at 1600, 800, and 400 nm, respectively [76], we find $\kappa/2\pi = 0.4$ MHz for SHG of telecom photons, and $\kappa/2\pi = 4$ MHz for SHG of 800 nm photons. The large coupling rates made possible by temporal trapping, when combined with absorption-limited losses, provide a pathway to $g/\kappa > 30$ at telecom wavelengths and $g/\kappa > 40$ at visible wavelengths. We compare these numbers against the current state of the art in a variety of material systems and waveguide geometries in Fig. 4. To date, the highest recorded g/κ based on optical nonlinearities is $g/\kappa \approx 10^{-2}$ in a 1550 nm pumped InGaP microresonator [26]. In principle, short-wavelength operation and reductions in resonator loss may push conventional cw-pumped nonlinear devices toward $g/\kappa = 0.1 - 1$. In contrast, the g/κ enabled by nonlinear resonators using temporal trapping may exceed these limits by two orders of magnitude.

4. CONCLUSION

In this work, we show that temporal trapping can realize strong photon–photon coupling by simultaneously leveraging both temporal and spatial field confinement. The energy gap created between the trapped mode and the remaining cavity modes suppresses undesired multimode interactions, realizing effective single-mode dynamics necessary for high-fidelity quantum gate operations. Our full-quantum simulations confirm that coherent nonlinear dynamics of temporally trapped ultrashort pulses can realize high-fidelity two-qubit entangling gates in a deterministic manner. This resolves the longstanding concern first raised by Shapiro that pulsed nonlinear optics cannot implement high-fidelity quantum gates [29,30].

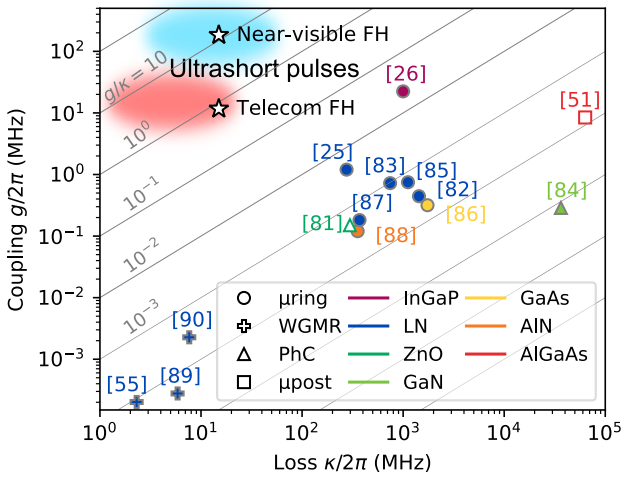

Fig. 4. Figure of merit g/κ shown for various material platforms and geometries, where the filled and unfilled markers represent experimental and theoretical results, respectively [25,26,51,55,81–90]. When g is not explicitly characterized, we use experimental measures of $\chi^{(2)}$ nonlinearity, e.g., SHG conversion efficiency, to estimate the coupling (see Supplement 1 for a full discussion and references). We assume critical coupling, phase-matching between the harmonics, and $\kappa_a = \kappa_b/2$ when the corresponding information is not provided. Stars represent numbers estimated for temporally trapped ultrashort pulses at telecom ($\lambda_a = 1560$ nm) and near-visible ($\lambda_a = 800$ nm) FH wavelengths.

Temporal trapping significantly brightens the prospects of achieving strong coupling in existing photonic platforms [40,41]. By reducing the effective cavity volume by the pulse duty cycle, g/κ can be increased by over an order of magnitude. Notably, numerical modeling based on realistic dispersion-engineered waveguide designs shows that $g/\kappa \sim 1$ is possible on existing TFLN platforms, and true strong coupling $g/\kappa \gg 1$ is plausible with realistic assumptions on wavelength scaling and loss, proposing a unique route towards deterministic optical quantum computation using ultrashort pulses.

Our generic prescription of using temporal trapping to realize enhanced single-mode nonlinear coupling can, in principle, be applied to a broad range of scenarios beyond discrete-variable NLOQC. For example, continuous-variable implementations of optical quantum computing [77,78] suffer from the same trade-off between linearity and determinism. Applied to these systems, strong photon–photon coupling can enable deterministic non-Gaussian gate operations and resource state preparations [79,80], circumventing the need for probabilistic implementations using measurement and feedback. Combined with the ability to manipulate temporal mode structures with optical pulse gating [66,67], deterministic quantum operations on arbitrary photon temporal modes could be realized. Our scheme is compatible with

intra-cavity time-multiplexing [32,33] and traveling-wave implementations, enabling unprecedented scalability, qubit uniformity, and operation bandwidth. We expect our work to shed light on the potential to harness ultrafast pulse dynamics for coherent quantum computation and engineering, guiding ongoing experimental and theoretical efforts towards this unique frontier of broadband quantum optics.

Funding. Army Research Office (W911NF-16-1-0086); National Science Foundation (CCF-1918549, PHY-2011363).

Acknowledgment. The authors thank NTT Research for financial and technical support. R. Y. is supported by a Stanford Q-FARM Ph.D. Fellowship and the Masason Foundation.

Disclosures. RY, EN, MJ, RH (P).

Data availability. Data underlying the results presented in this paper are not publicly available at this time but may be obtained from the authors upon reasonable request.

Supplemental document. See Supplement 1 for supporting content.

REFERENCES

1. H.-L. Yin, T.-Y. Chen, Z.-W. Yu, H. Liu, L.-X. You, Y.-H. Zhou, S.-J. Chen, Y. Mao, M.-Q. Huang, W.-J. Zhang, H. Chen, M. J. Li, D. Nolan, F. Zhou, X. Jiang, Z. Wang, Q. Zhang, X.-B. Wang, and J.-W. Pan, "Measurement-device-independent quantum key distribution over a 404 km optical fiber," Phys. Rev. Lett. **117**, 190501 (2016).
2. H. J. Kimble, "The quantum internet," Nature **453**, 1023–1030 (2008).
3. The LIGO Scientific Collaboration, "Enhanced sensitivity of the LIGO gravitational wave detector by using squeezed states of light," Nat. Photonics **7**, 613–619 (2013).
4. N. Treps, U. Andersen, B. Buchler, P. K. Lam, A. Maître, H. A. Bachor, and C. Fabre, "Surpassing the standard quantum limit for optical imaging using nonclassical multimode light," Phys. Rev. Lett. **88**, 203601 (2002).
5. J. L. O'Brien, A. Furusawa, and J. Vučković, "Photonic quantum technologies," Nat. Photonics **3**, 687–695 (2009).
6. W. Asavanant, Y. Shiozawa, S. Yokoyama, B. Charoensombutamon, H. Emura, R. N. Alexander, S. Takeda, J. Yoshikawa, N. C. Menicucci, H. Yonezawa, and A. Furusawa, "Generation of time-domain-multiplexed two-dimensional cluster state," Science **366**, 373–376 (2019).
7. J. L. O'Brien, "Optical quantum computing," Science **318**, 1567–1570 (2007).
8. E. Knill, R. Laflamme, and G. J. Milburn, "A scheme for efficient quantum computation with linear optics," Nature **409**, 46–52 (2001).
9. E. Knill, "Quantum gates using linear optics and postselection," Phys. Rev. A **66**, 052306 (2002).
10. R. Raussendorf and H. J. Briegel, "A one-way quantum computer," Phys. Rev. Lett. **86**, 5188 (2001).
11. M. A. Nielsen, "Optical quantum computation using cluster states," Phys. Rev. Lett. **93**, 040503 (2004).
12. C. Reimer, S. Sciara, P. Roztocki, M. Islam, L. Romero Cortés, Y. Zhang, B. Fischer, S. Loranger, R. Kashyap, A. Cino, S. T. Chu, B. E. Little, D. J. Moss, L. Caspani, W. J. Munro, J. Azaña, M. Kues, and R. Morandotti, "High-dimensional one-way quantum processing implemented on D-level cluster states," Nat. Phys. **15**, 148–153 (2019).
13. S. Slussarenko and G. J. Pryde, "Photonic quantum information processing: a concise review," Appl. Phys. Rev. **6**, 041303 (2019).
14. Y. Li, P. C. Humphreys, G. J. Mendoza, and S. C. Benjamin, "Resource costs for fault-tolerant linear optical quantum computing," Phys. Rev. X **5**, 041007 (2015).
15. P. Kok, W. J. Munro, K. Nemoto, T. C. Ralph, J. P. Dowling, and G. J. Milburn, "Linear optical quantum computing with photonic qubits," Rev. Mod. Phys. **79**, 135 (2007).
16. T. Rudolph, "Why I am optimistic about the silicon-photonic route to quantum computing," APL Photon. **2**, 030901 (2017).
17. I. L. Chuang and Y. Yamamoto, "Simple quantum computer," Phys. Rev. A **52**, 3489 (1995).
18. N. K. Langford, S. Ramelow, R. Prevedel, W. J. Munro, G. J. Milburn, and A. Zeilinger, "Efficient quantum computing using coherent photon conversion," Nature **478**, 360–363 (2011).
19. T. Yoshie, A. Scherer, J. Hendrickson, G. Khitrova, H. Gibbs, G. Rupper, C. Ell, O. Shchekin, and D. Deppe, "Vacuum Rabi splitting with a single quantum dot in a photonic crystal nanocavity," Nature **432**, 200–203 (2004).
20. K. M. Birnbaum, A. Boca, R. Miller, A. D. Boozer, T. E. Northup, and H. J. Kimble, "Photon blockade in an optical cavity with one trapped atom," Nature **436**, 87–90 (2005).
21. D. Englund, A. Faraon, I. Fushman, N. Stoltz, P. Petroff, and J. Vučković, "Controlling cavity reflectivity with a single quantum dot," Nature **450**, 857–861 (2007).
22. B. Hacker, S. Welte, G. Rempe, and S. Ritter, "A photon–photon quantum gate based on a single atom in an optical resonator," Nature **536**, 193–196 (2016).
23. A. Boca, R. Miller, K. M. Birnbaum, A. D. Boozer, J. McKeever, and H. J. Kimble, "Observation of the vacuum Rabi spectrum for one trapped atom," Phys. Rev. Lett. **93**, 233603 (2004).
24. M. Zhang, C. Wang, R. Cheng, A. Shams-Ansari, and M. Lončar, "Monolithic ultra-high-Q lithium niobate microring resonator," Optica **4**, 1536–1537 (2017).
25. J. Lu, M. Li, C.-L. Zou, A. Al Sayem, and H. X. Tang, "Toward 1% single photon nonlinearity with periodically-poled lithium niobate microring resonators," Optica **7**, 1654–1659 (2020).
26. M. Zhao and K. Fang, "InGaP quantum nanophotonic integrated circuits with 1.5% nonlinearity-to-loss ratio," Optica **9**, 258–263 (2022).
27. G. P. Agrawal, "Nonlinear fiber optics," in *Nonlinear Science at the Dawn of the 21st Century* (Springer, 2000), pp. 195–211.
28. M. Jankowski, J. Mishra, and M. M. Fejer, "Dispersion-engineered $\chi^{(2)}$ nanophotonics: a flexible tool for nonclassical light," J. Phys. Photon. **3**, 042005 (2021).
29. J. H. Shapiro, "Single-photon Kerr nonlinearities do not help quantum computation," Phys. Rev. A **73**, 062305 (2006).
30. J. H. Shapiro and M. Razavi, "Continuous-time cross-phase modulation and quantum computation," New J. Phys. **9**, 16 (2007).
31. G. J. Milburn, "Quantum optical Fredkin gate," Phys. Rev. Lett. **62**, 2124 (1989).
32. T. Inagaki, K. Inaba, R. Hamerly, K. Inoue, Y. Yamamoto, and H. Takesue, "Large-scale Ising spin network based on degenerate optical parametric oscillators," Nat. Photonics **10**, 415–419 (2016).
33. S. Takeda and A. Furusawa, "Universal quantum computing with measurement-induced continuous-variable gate sequence in a loop-based architecture," Phys. Rev. Lett. **119**, 120504 (2017).
34. A. Crespi, R. Ramponi, R. Osellame, L. Sansoni, I. Bongioanni, F. Sciarrino, G. Vallone, and P. Mataloni, "Integrated photonic quantum gates for polarization qubits," Nat. Commun. **2**, 566 (2011).
35. P. C. Humphreys, B. J. Metcalf, J. B. Spring, M. Moore, X.-M. Jin, M. Barbieri, W. S. Kolthammer, and I. A. Walmsley, "Linear optical quantum computing in a single spatial mode," Phys. Rev. Lett. **111**, 150501 (2013).
36. X. Qiang, X. Zhou, J. Wang, C. M. Wilkes, T. Loke, S. O'Gara, L. Kling, G. D. Marshall, R. Santagati, T. C. Ralph, J. B. Wang, J. L. O'Brien, M. G. Thompson, and J. C. F. Matthews, "Large-scale silicon quantum photonics implementing arbitrary two-qubit processing," Nat. Photonics **12**, 534–539 (2018).
37. J. L. O'Brien, G. J. Pryde, A. G. White, T. C. Ralph, and D. Branning, "Demonstration of an all-optical quantum controlled-NOT gate," Nature **426**, 264–267 (2003).
38. C. K. Hong, Z. Y. Ou, and L. Mandel, "Measurement of subpicosecond time intervals between two photons by interference," Phys. Rev. Lett. **59**, 2044 (1987).
39. A. P. VanDevender and P. G. Kwiat, "High-speed transparent switch via frequency upconversion," Opt. Express **15**, 4677–4683 (2007).
40. W. T. M. Irvine, K. Hennessy, and D. Bouwmeester, "Strong coupling between single photons in semiconductor microcavities," Phys. Rev. Lett. **96**, 057405 (2006).
41. A. Majumdar and D. Gerace, "Single-photon blockade in doubly resonant nanocavities with second-order nonlinearity," Phys. Rev. B **87**, 235319 (2013).
42. Q. Quan and M. Lončar, "Deterministic design of wavelength scale, ultra-high Q photonic crystal nanobeam cavities," Opt. Express **19**, 18529–18542 (2011).
43. T. Asano and S. Noda, "Iterative optimization of photonic crystal nanocavity designs by using deep neural networks," Nanophotonics **8**, 2243–2256 (2019).

44. H. Sekoguchi, Y. Takahashi, T. Asano, and S. Noda, "Photonic crystal nanocavity with a Q-factor of 9 million," Opt. Express **22**, 916–924 (2014).
45. M. Minkov and V. Savona, "Automated optimization of photonic crystal slab cavities," Sci. Rep. **4**, 5124 (2014).
46. T. Asano, Y. Ochi, Y. Takahashi, K. Kishimoto, and S. Noda, "Photonic crystal nanocavity with a Q factor exceeding eleven million," Opt. Express **25**, 1769–1777 (2017).
47. D. Dodane, J. Bourderionnet, S. Combrié, and A. de Rossi, "Fully embedded photonic crystal cavity with Q=0.6 million fabricated within a full-process CMOS multiproject wafer," Opt. Express **26**, 20868–20877 (2018).
48. Y. Taguchi, Y. Takahashi, Y. Sato, T. Asano, and S. Noda, "Statistical studies of photonic heterostructure nanocavities with an average Q factor of three million," Opt. Express **19**, 11916–11921 (2011).
49. K. Rivoire, S. Buckley, and J. Vučković, "Multiply resonant photonic crystal nanocavities for nonlinear frequency conversion," Opt. Express **19**, 22198–22207 (2011).
50. M. Minkov, D. Gerace, and S. Fan, "Doubly resonant $\chi^{(2)}$ nonlinear photonic crystal cavity based on a bound state in the continuum," Optica **6**, 1039–1045 (2019).
51. Z. Lin, X. Liang, M. Lončar, S. G. Johnson, and A. W. Rodriguez, "Cavity-enhanced second-harmonic generation via nonlinear-overlap optimization," Optica **3**, 233–238 (2016).
52. Z. Lin, M. Lončar, and A. W. Rodriguez, "Topology optimization of multi-track ring resonators and 2D microcavities for nonlinear frequency conversion," Opt. Lett. **42**, 2818–2821 (2017).
53. A. Shams-Ansari, G. Huang, L. He, M. Churaev, P. Kharel, Z. Tan, J. Holzgrafe, R. Cheng, D. Zhu, J. Liu, B. Desiatov, M. Zhang, T. J. Kippenberg, and M. Lončar, "Probing the limits of optical loss in ion-sliced thin-film lithium niobate," in *CLEO: Science and Innovations* (Optical Society of America, 2021), paper STh4J–4.
54. R. Gao, H. Zhang, F. Bo, W. Fang, Z. Hao, N. Yao, J. Lin, J. Guan, L. Deng, M. Wang, L. Qiao, and Y. Cheng, "Broadband highly efficient nonlinear optical processes in on-chip integrated lithium niobate microdisk resonators of Q-factor above 10^8," New J. Phys. **23**, 123027 (2021).
55. R. Gao, N. Yao, J. Guan, L. Deng, J. Lin, M. Wang, L. Qiao, W. Fang, and Y. Cheng, "Lithium niobate microring with ultra-high Q factor above 10^8," Chin. Opt. Lett. **20**, 011902 (2022).
56. V. S. Ilchenko, A. A. Savchenkov, A. B. Matsko, and L. Maleki, "Nonlinear optics and crystalline whispering gallery mode cavities," Phys. Rev. Lett. **92**, 043903 (2004).
57. D. Serkland, R. Eckardt, and R. Byer, "Continuous-wave total-internal-reflection optical parametric oscillator pumped at 1064 nm," Opt. Lett. **19**, 1046–1048 (1994).
58. A. A. Savchenkov, V. S. Ilchenko, A. B. Matsko, and L. Maleki, "Kilohertz optical resonances in dielectric crystal cavities," Phys. Rev. A **70**, 051804 (2004).
59. J. R. Schwesyg, M. C. C. Kajiyama, M. Falk, D. H. Jundt, K. Buse, and M. M. Fejer, "Light absorption in undoped congruent and magnesium-doped lithium niobate crystals in the visible wavelength range," Appl. Phys. B **100**, 109–115 (2010).
60. S. Ramelow, A. Farsi, Z. Vernon, S. Clemmen, X. Ji, J. E. Sipe, M. Liscidini, M. Lipson, and A. L. Gaeta, "Strong nonlinear coupling in a Si_3N_4 ring resonator," Phys. Rev. Lett. **122**, 153906 (2019).
61. N. Quesada, L. G. Helt, M. Menotti, M. Liscidini, and J. E. Sipe, *Beyond Photon Pairs: Nonlinear Quantum Photonics in the High-Gain Regime* (2021).
62. L. A. Lugiato and R. Lefever, "Spatial dissipative structures in passive optical systems," Phys. Rev. Lett. **58**, 2209 (1987).
63. K. Nemoto and W. J. Munro, "Nearly deterministic linear optical controlled-not gate," Phys. Rev. Lett. **93**, 250502 (2004).
64. K. Fukui, M. Endo, W. Asavanant, A. Sakaguchi, J. Yoshikawa, and A. Furusawa, "Generating the Gottesman-Kitaev-Preskill qubit using a cross-Kerr interaction between squeezed light and Fock states in optics," Phys. Rev. A **105**, 022436 (2022).
65. H. Carmichael, *An Open Systems Approach to Quantum Optics*, Lectures presented at the Université Libre de Bruxelles, October 28 to November 4, 1991 (Springer, 2009), Vol. **18**.
66. B. Brecht, D. V. Reddy, C. Silberhorn, and M. G. Raymer, "Photon temporal modes: a complete framework for quantum information science," Phys. Rev. X **5**, 041017 (2015).
67. B. Brecht, A. Eckstein, A. Christ, and C. Silberhorn, "From quantum pulse gate to quantum pulse shaper—engineered frequency conversion in nonlinear optical waveguides," New J. Phys. **13**, 065029 (2011).
68. A. Eckstein, A. Christ, P. J. Mosley, and C. Silberhorn, "Highly efficient single-pass source of pulsed single-mode twin beams of light," Phys. Rev. Lett. **106**, 013603 (2011).
69. M. Heuck, K. Jacobs, and D. R. Englund, "Photon-photon interactions in dynamically coupled cavities," Phys. Rev. A **101**, 042322 (2020).
70. M. Heuck, K. Jacobs, and D. R. Englund, "Controlled-phase gate using dynamically coupled cavities and optical nonlinearities," Phys. Rev. Lett. **124**, 160501 (2020).
71. M. Zhang, C. Wang, Y. Hu, A. Shams-Ansari, T. Ren, S. Fan, and M. Lončar, "Electronically programmable photonic molecule," Nat. Photonics **13**, 36 (2019).
72. D. Zhu, L. Shao, M. Yu, R. Cheng, B. Desiatov, C. J. Xin, Y. Hu, J. Holzgrafe, S. Ghosh, A. Shams-Ansari, E. Puma, N. Sinclair, C. Reimer, M. Zhang, and M. Lončar, "Integrated photonics on thin-film lithium niobate," Adv. Opt. Photon. **13**, 242–352 (2021).
73. T. Park, H. S. Stokowski, V. Ansari, T. P. McKenna, A. Y. Hwang, M. M. Fejer, and A. H. Safavi-Naeini, "High efficiency second harmonic generation of blue light on thin film lithium niobate," Opt. Lett. **47**, 2706–2709 (2022).
74. R. Bhatt, I. Bhaumik, S. Ganesamoorthy, A. K. Karnal, M. K. Swami, H. S. Patel, and P. K. Gupta, "Urbach tail and bandgap analysis in near stoichiometric $LiNbO_3$ crystals," Phys. Status Solidi A **209**, 176–180 (2011).
75. B. Desiatov, A. Shams-Ansari, M. Zhang, C. Wang, and M. Lončar, "Ultra-low-loss integrated visible photonics using thin-film lithium niobate," Optica **6**, 380–384 (2019).
76. M. Leidinger, S. Fieberg, N. Waasem, F. Kühnemann, K. Buse, and I. Breunig, "Comparative study on three highly sensitive absorption measurement techniques characterizing lithium niobate over its entire transparent spectral range," Opt. Express **23**, 21690–21705 (2015).
77. N. C. Menicucci, P. van Loock, M. Gu, C. Weedbrook, T. C. Ralph, and M. A. Nielsen, "Universal quantum computation with continuous-variable cluster states," Phys. Rev. Lett. **97**, 110501 (2006).
78. S. Takeda and A. Furusawa, "Toward large-scale fault-tolerant universal photonic quantum computing," APL Photon. **4**, 060902 (2019).
79. R. Yanagimoto, T. Onodera, E. Ng, L. G. Wright, P. L. McMahon, and H. Mabuchi, "Engineering a Kerr-based deterministic cubic phase gate via Gaussian operations," Phys. Rev. Lett. **124**, 240503 (2020).
80. Y. Zheng, O. Hahn, P. Stadler, P. Holmvall, F. Quijandría, A. Ferraro, and G. Ferrini, "Gaussian conversion protocols for cubic phase state generation," PRX Quantum **2**, 010327 (2021).
81. J. A. Medina-Vázquez, E. Y. González-Ramírez, and J. G. Murillo-Ramírez, "Photonic crystal meso-cavity with double resonance for second-harmonic generation," J. Phys. B **54**, 245401 (2022).
82. J.-Y. Chen, C. Tang, M. Jin, Z. Li, Z. Ma, H. Fan, S. Kumar, Y. M. Sua, and Y.-P. Huang, "Efficient frequency doubling with active stabilization on chip," Laser Photon. Rev. **15**, 2100091 (2021).
83. J.-Y. Chen, Z. Li, Z. Ma, C. Tang, H. Fan, Y. M. Sua, and Y.-P. Huang, *Photon Conversion and Interaction on Chip* (2021).
84. J. Wang, M. Clementi, M. Minkov, A. Barone, J.-F. Carlin, N. Grandjean, D. Gerace, S. Fan, M. Galli, and R. Houdré, "Doubly resonant second-harmonic generation of a vortex beam from a bound state in the continuum," Optica **7**, 1126–1132 (2020).
85. Z. Ma, J.-Y. Chen, Z. Li, C. Tang, Y. M. Sua, H. Fan, and Y.-P. Huang, "Ultrabright quantum photon sources on chip," Phys. Rev. Lett. **125**, 263602 (2020).
86. L. Chang, A. Boes, P. Pintus, J. D. Peters, M. Kennedy, X.-W. Guo, N. Volet, S.-P. Yu, S. B. Papp, and J. E. Bowers, "Strong frequency conversion in heterogeneously integrated GaAs resonators," APL Photon. **4**, 036103 (2019).
87. J.-Y. Chen, Z.-H. Ma, Y. M. Sua, Z. Li, C. Tang, and Y.-P. Huang, "Ultra-efficient frequency conversion in quasi-phase-matched lithium niobate microrings," Optica **6**, 1244–1245 (2019).
88. A. W. Bruch, X. Liu, X. Guo, J. B. Surya, Z. Gong, L. Zhang, J. Wang, J. Yan, and H. X. Tang, "17000%/W second-harmonic conversion efficiency in single-crystalline aluminum nitride microresonators," Appl. Phys. Lett. **113**, 131102 (2018).
89. J. U. Fürst, D. V. Strekalov, D. Elser, M. Lassen, U. L. Andersen, C. Marquardt, and G. Leuchs, "Naturally phase-matched second-harmonic generation in a whispering-gallery-mode resonator," Phys. Rev. Lett. **104**, 153901 (2010).
90. J. U. Fürst, D. V. Strekalov, D. Elser, A. Aiello, U. L. Andersen, C. Marquardt, and G. Leuchs, "Low-threshold optical parametric oscillations in a whispering gallery mode resonator," Phys. Rev. Lett. **105**, 263904 (2010).